Journal of Naval Architecture and Marine Engineering
December, 2007
DOI: 10.3329/jname.v4i2.991 http://jname.8m.net

FLOW THROUGH A HELICAL PIPE WITH RECTANGULAR CROSS-SECTION

MD. MAHMUD ALAM[1], DELOWARA BEGUM[1] AND K. YAMAMOTO[2]

[1]Mathematics Discipline, Khulna University, Khulna-9208, Bangladesh, [2]Department of Mechanical Engineering, Okayama University, Okayama 700, Japan

Abstract

The effects of torsion, aspect ratio and curvature on the flow in a helical pipe of rectangular cross- section are studied by introducing a non-orthogonal helical coordinate system. Spectral method is applied as main tool for numerical approach where Chebyshev polynomial is used. The numerical calculations are obtained by the iterative method. The calculations are carried out for $0\leq \delta \leq 0.02$, $1\leq \lambda \leq 2.85$, $1\leq \gamma \leq 2.4$, at $D_n = 50$ & 100 respectively, where δ is the non-dimensional curvature, λ the torsion parameter, γ the aspect ratio and D_n the pressure driven parameter (Dean number)..

Key words: *Spectral method, non-orthogonal helical coordinate system, Chebyshev polynomial, steady fluid flow, helical pipe, Dean number*

1. Introduction

The curved geometry of helical pipe is important from both industrial and academic standpoint. The helical square pipe has been used extensively in various industrial applications to enhance the rate of heat, mass and momentum transfer. In order to improve the performance of these devices, an accurate and reliable analysis of the flow in the helical pipe is necessary, which can also be used as the basis for studying the flow in other devices, such as screw pumps, heat exchangers, and the passage between the blades of gas turbines or centrifugal compressors. The shape of a helical rectangular duct is as shown in Fig. 1 and it is determined by the dimensionless curvature δ and torsionτ. The torsion and curvature are defined, respectively, as $\tau = \dfrac{\alpha' a}{r_0'^2 + \alpha'^2}$ and $\delta = \dfrac{r_0' a}{r_0'^2 + \alpha'^2}$, where α is the width of the cross section of the helical pipe, $2\pi\alpha'$ the pitch of the helical pipe and r_0' the radius of the tube that the helical pipe is wound around. The curvature δ and the torsion τ of the centre line of the pipe characterize the particular kind of a pipe. For example, for a toroidal pipe, δ is constant and τ is zero, and for helical pipe, both τ and δ are finite and nonzero. The torsion gives rise to the so-called pitch of the pipe, $2\pi\alpha'$, as shown in Fig. 1**.** The curvature induces centrifugal force acting on the flow in the pipe. The action of the centrifugal force in a toroidal pipe has been studied by Joseph et al.(1975), Cheng et al.(1976), Ghia and Sokhey(1977) and Winters(1987).

A finite torsion generally makes the co-ordinate system non-orthogonal. Wang(1981) for the first time handled the problem of flow in a helical circular pipe using a non-orthogonal helical co-ordinate system. The flow in the helical pipe has been studied for circular (Manlapaz et al.(1980); Wang(1981); Murata et al.(1981); Chen and Fan(1986); Kao(1987); Xie(1990)) cross sections. Yamamoto et al. (2000) first studied the flow in rotating helical pipe with circular cross-section. Very few numbers of studies regarding the torsion effect on the flow in a helical pipe of rectangular cross-section with large aspect ratio were studied.

Hence, our object is to establish a set of mathematical equations in tensor form that can describe the flow through a helical duct. The non-orthogonal helical co-ordinate system (r', s', t') has been used in the present problem. Spectral method is used as a tool to solve the non-linear partial differential equations involved. The obtained non-linear algebraic equations are solved by iterative method. The

role of curvature, aspect ratio and torsion of the helical duct is investigated.

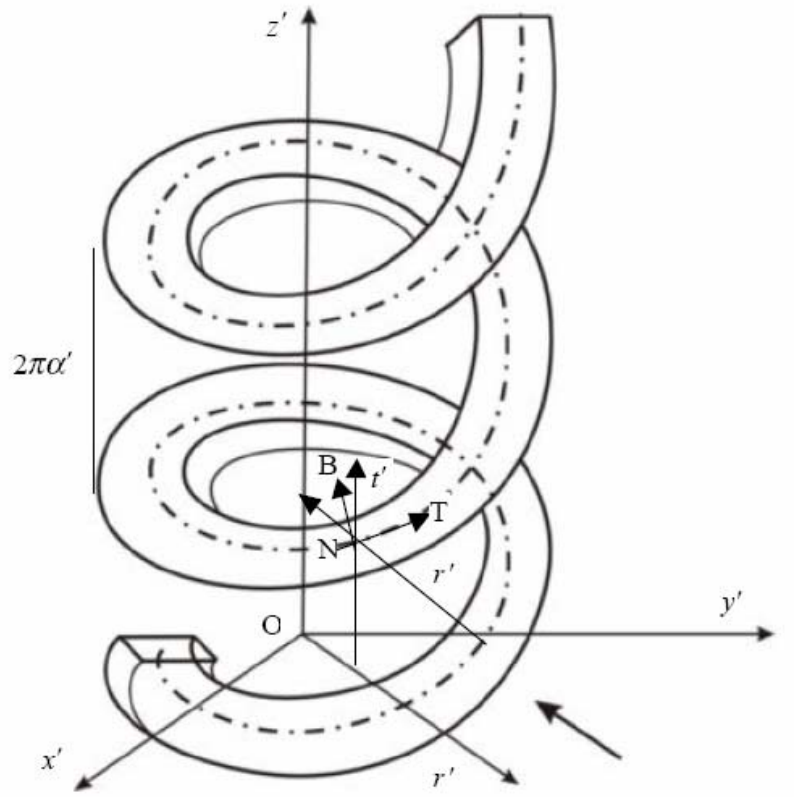

Fig.1 Helical pipe with rectangular cross-section and coordinate system.

2. Governing Equations

A coordinate system that is suitable for describing fluid flow through a helical pipe (with square cross-section) is helical coordinate system, as shown in Fig.1, which is a non-orthogonal coordinate system. Any point in the helical pipe can be defined by a Cartesian position vector R, which is a function of the co-ordinate system (r', s', t') as shown in Fig. 1, where r' is the radial co-ordinate, s' is the co-ordinate along the centre line of the cross-section and t' is the co-ordinate parallel to the center line of the helix. The position vector R at any arbitrary point on the centerline is expressed as: $R = r'\cos s'\hat{i} + r'\sin s'\hat{j} + (\alpha' s' + t')k'$.

Along the centerline, the unit tangent, normal and binormal vectors are mutually orthogonal and denoted as T, N and B respectively. The helical coordinate system (r', s', t') is constructed with the co-ordinates (r', t'), defined by the plane of N and B, and the third coordinate s' along the axial direction of the helical pipe of square cross section.

Following Serret-Frenet formulas have been used for finding the curvature and torsion:

$$T = \frac{dR}{ds}, N = \frac{1}{\kappa'}\frac{dT}{ds}, \tau' B - \kappa' T = \frac{dN}{ds}, -\tau' N = \frac{dB}{ds}, B = T \wedge N$$

Now the co-ordinates (r', s', t') are transferred to $(\bar{r}', s', t')$, where $r' = r_0' + \bar{r}'$. The dependent and independent variables are then normalized as follows:

$$r_0' + \bar{r}' = (\delta_0^{-1} + \eta)a = \alpha a,\ u' = \frac{\upsilon}{a}u,\ v' = \frac{\upsilon}{a}\frac{v}{\sqrt{2\delta}},\ w' = \frac{\upsilon}{a}w,\ t' = ta,\ p' = \rho\frac{\upsilon^2}{a^2}p,\ \delta = \kappa' a,\ \tau = \tau' a = \delta\lambda,$$

$$\delta_0^{-1} = \frac{1}{\delta(1+\lambda^2)},\ \alpha = \frac{\lambda}{\delta(1+\lambda^2)},\ \gamma = \frac{b'\sqrt{1+\lambda^2}}{a},\ s' = \frac{s\delta}{a^2}$$

where the variables with prime are the dimensional quantities. Assuming that the flow is steady and fully developed and hence the flow velocity is independent of s and the generalized Navier Stokes equations can be put in the following non-dimensional forms;

in the η direction;

$$u\frac{\partial u}{\partial \eta} + w\frac{\partial u}{\partial t} - \frac{(1+\eta\delta_0)\delta_0 v^2}{2\delta[(1+\eta\delta_0)^2 + \alpha^2{\delta_0}^2]} = -\frac{\partial p}{\partial \eta}\frac{\partial^2 u}{\partial \eta^2} + \left(1 + \frac{\alpha^2\delta_0^2}{(1+\eta\delta_0)^2}\right)\frac{\partial^2 u}{\partial t^2} + \frac{\delta_0}{1+\eta\delta_0}\frac{\partial u}{\partial \eta} +$$

$$\frac{\alpha\delta_0^2}{\sqrt{2\delta}(1+\eta\delta_0)}\frac{\partial}{\partial t}\left(\frac{v}{\sqrt{(1+\eta\delta_0)^2 + \alpha^2\delta_0^2}}\right) - \frac{u\delta_0^2}{(1+\eta\delta_0^2)} \tag{1}$$

in the *s* direction;

$$u\frac{\partial}{\partial \eta}\left(\frac{v}{\sqrt{(1+\eta\delta_0)^2 + \alpha^2\delta_0^2}}\right) + w\frac{\partial}{\partial t}\left(\frac{v}{\sqrt{(1+\eta\delta_0)^2 + \alpha^2\delta_0^2}}\right) + \frac{2uv\delta_0}{(1+\eta\delta_0)\sqrt{(1+\eta\delta_0)^2 + \alpha^2\delta_0^2}}$$

$$= \frac{\delta_0 D_n}{\delta(1+\eta\delta_0)^2} + \frac{\sqrt{2\delta\alpha\delta_0}}{(1+\eta\delta_0)^2}\frac{\partial p}{\partial t} + \frac{\partial^2}{\partial \eta^2}\left(\frac{v}{\sqrt{(1+\eta\delta_0)^2 + \alpha^2\delta_0^2}}\right) + \left(1 + \frac{\alpha^2\delta_0^2}{(1+\eta\delta_0)^2}\right)\frac{\partial^2}{\partial t^2}\left(\frac{v}{\sqrt{(1+\eta\delta_0)^2 + \alpha^2\delta_0^2}}\right)$$

$$+ \frac{3\delta_0}{(1+\eta\delta_0)}\frac{\partial}{\partial \eta}\left(\frac{v}{\sqrt{(1+\eta\delta_0)^2 + \alpha^2\delta_0^2}}\right) - \frac{\sqrt{2\delta}\alpha\delta_0^2}{(1+\eta\delta_0)^3}\frac{\partial u}{\partial t} \tag{2}$$

in the *t* direction;

$$u\frac{\partial w}{\partial \eta} + w\frac{\partial w}{\partial t} - \frac{2uv\alpha\delta_0^2}{\sqrt{2\delta}(1+\eta\delta_0)\sqrt{(1+\eta\delta_0)^2 + \alpha^2\delta_0^2}} = -\frac{\alpha\delta_0^2 D_n}{\delta\sqrt{2\delta}(1+\eta\delta_0)^2} - \left(1 + \frac{\alpha^2\delta_0^2}{(1+\eta\delta_0)^2}\right)\frac{\partial p}{\partial t}$$

$$+ \left(1 + \frac{\alpha^2\delta_0^2}{(1+\eta\delta_0)^2}\right)\frac{\partial^2 w}{\partial t^2} - \frac{2\alpha\delta_0^2}{\sqrt{2\delta}(1+\eta\delta_0)^2 + \alpha^2\delta_0^2} + \left(\frac{\delta_0}{1+\eta\delta_0}\right)\frac{\partial w}{\partial \eta} + \left(\frac{\alpha^2\delta_0^3}{(1+\eta\delta_0)^3}\right)\frac{\partial u}{\partial t} \tag{3}$$

the continuity equation;

$$\frac{\partial u}{\partial \eta} + \frac{\partial w}{\partial t} + \frac{u\delta_0}{(1+\eta\delta_0)} = 0, \tag{4}$$

where $D_n = \frac{a^3}{\mu\upsilon}\sqrt{2\delta}G$ (Dean number), μ the viscosity, $G = -\frac{\partial P}{\partial s'}$ the constant pressure gradient along the duct axis, $p\ (\eta, t)$ the pressure in a cross-section and is related with the non-dimensional pressure P by $P = -Gs + p(\eta, t)$.

We further introduce the new variable $\xi = \frac{t}{\gamma\sqrt{1+\lambda^2}}$ and the stream function ψ such that

$$u = \frac{1}{1+\eta\delta_0}\frac{1}{\gamma\sqrt{1+\lambda^2}}\frac{\partial\psi}{\partial\xi}, w = -\frac{1}{1+\eta\delta_0}\frac{\partial\psi}{\partial\eta}, \tag{5}$$

which satisfies the continuity equation (4).

The corresponding boundary conditions are $u = v = w = 0$ at $\eta = \pm 1$ and $\xi = \pm\gamma\sqrt{1+\lambda^2}$. The assumption of a fully developed flow means that except for the pressure derivative all s derivatives are

set to zero. Eliminating p in the resulting equations (1)-(5) and we have the following equations for ψ and v, which are used for numerical calculations,

$$\frac{1+\eta\delta_0}{\sqrt{(1+\eta\delta_0)^2+\lambda^2}}\frac{1}{\gamma}\left(\frac{\partial\psi}{\partial\xi}\frac{\partial v}{\partial\eta}-\frac{\partial\psi}{\partial\eta}\frac{\partial v}{\partial\xi}\right)+\frac{1}{\gamma}\left(\frac{2\delta_0}{\sqrt{(1+\eta\delta_0)^2+\lambda^2}}-\frac{\delta_0(1+\eta\delta_0)^2}{\left\{(1+\eta\delta_0)^2+\lambda^2\right\}^{3/2}}\frac{\partial\psi}{\partial\xi}v\right)$$

$$=D_n(1+\lambda^2)+\sqrt{2\delta}\frac{\lambda}{\gamma}\frac{\partial p}{\partial\xi}+\frac{(1+\eta\delta_0)^2}{\sqrt{(1+\eta\delta_0)^2+\lambda^2}}\frac{\partial^2 v}{\partial\eta^2}+\frac{1}{\gamma^2}\sqrt{(1+\eta\delta_0)^2+\lambda^2}\frac{\partial^2 v}{\partial\xi^2}+\left[\frac{3\delta_0(1+\eta\delta_0)}{\sqrt{(1+\eta\delta_0)^2+\lambda^2}}\right.$$

$$\left.-\frac{2\delta_0(1+\eta\delta_0)^3}{\left\{(1+\eta\delta_0)^2+\lambda^2\right\}^{3/2}}\right]\frac{\partial v}{\partial\eta}+\left[\frac{3(1+\eta\delta_0)^4\delta_0^2}{\left\{(1+\eta\delta_0)^2+\lambda^2\right\}^{5/2}}-\frac{4(1+\eta\delta_0)^2\delta_0^2}{\left\{(1+\eta\delta_0)^2+\lambda^2\right\}^{3/2}}\right]v-\frac{\sqrt{2\delta}\lambda\delta_0}{(1+\eta\delta_0)^2}\frac{1}{\gamma^2}\frac{\partial^2\psi}{\partial\xi^2} \qquad (6)$$

$$\frac{(1+\eta\delta_0)}{(1+\eta\delta_0)^2+\lambda^2}\frac{1}{\gamma}\left(-\frac{\partial\psi}{\partial\xi}\frac{\partial^3\psi}{\partial\eta^3}+\frac{\partial\psi}{\partial\eta}\frac{\partial^3\psi}{\partial\eta^2\partial\xi}+\frac{3\delta_0}{(1+\eta\delta_0)}\frac{\partial^2\psi}{\partial\eta^2}\frac{\partial\psi}{\partial\xi}-\frac{3\delta_0^2}{(1+\eta\delta_0)^2}\frac{\partial\psi}{\partial\xi}\frac{\partial\psi}{\partial\eta}-\frac{\delta_0}{1+\eta\delta_0}\frac{\partial^2\psi}{\partial\eta\partial\xi}\frac{\partial\psi}{\partial\eta}\right)+$$

$$\left[-\frac{\partial\psi}{\partial\xi}\frac{\partial^2\psi}{\partial\eta^2}+\frac{\delta_0}{1+\eta\delta_0}\frac{\partial\psi}{\partial\xi}\frac{\partial\psi}{\partial\eta}+\frac{\partial\psi}{\partial\eta}\frac{\partial^{2\psi}}{\partial\eta\partial\xi}\right]\frac{1}{\gamma}\frac{2\delta_0\lambda^2}{\left\{(1+\eta\delta_0)^2+\lambda^2\right\}^2}-\frac{2\lambda\delta_0(1+\eta\delta_0)}{\sqrt{2\delta}\left\{(1+\eta\delta_0)^2+\lambda^2\right\}^{3/2}}\frac{1}{\gamma}\left(\frac{\partial^2\psi}{\partial\eta\partial\xi}v\right.$$

$$\left.-\frac{\delta_0}{1+\eta\delta_0}\frac{\partial\psi}{\partial\xi}v+\frac{\partial\psi}{\partial\xi}\frac{\partial v}{\partial\eta}\right)-\frac{2\lambda\delta_0^2}{\sqrt{2\delta}}\frac{1}{\gamma}\frac{\partial\psi}{\partial\xi}v\left[\frac{\lambda^2-2(1+\eta\delta_0)^2}{\left\{(1+\eta\delta_0)^2+\lambda^2\right\}^{5/2}}\right]=\frac{2D_n\lambda(1+\lambda^2)\delta_0}{\sqrt{2\delta}}\frac{(1+\eta\delta_0)^2}{\left\{(1+\eta\delta_0)^2+\lambda^2\right\}^2}$$

$$-(1+\eta\delta_0)\frac{1}{\gamma}\frac{\partial^2 p}{\partial\eta\partial\xi}-\frac{(1+\eta\delta_0)^2}{(1+\eta\delta_0)^2+\lambda^2}\frac{\partial^4\psi}{\partial\eta^4}-\frac{(1+\eta\delta_0)}{(1+\eta\delta_0)^2+\lambda^2}\left[-3\delta_0\frac{\partial^3\psi}{\partial\eta^3}+\frac{6\delta_0^2}{(1+\eta\delta_0)}\frac{\partial^2\psi}{\partial\eta^2}-\frac{6\delta_0^3}{(1+\eta\delta_0)^2}\frac{\partial\psi}{\partial\eta}\right]$$

$$-\frac{2\delta_0\lambda^2(1+\eta\delta_0)}{\left\{(1+\eta\delta_0)^2+\lambda^2\right\}^2}\left[\frac{\partial^3\psi}{\partial\eta^3}-\frac{2\delta_0}{(1+\eta\delta_0)}\frac{\partial^2\psi}{\partial\eta^2}+\frac{2\delta_0^2}{(1+\eta\delta_0)^2}\frac{\partial\psi}{\partial\eta}\right]-\frac{1}{\gamma^2}\frac{\partial^4\psi}{\partial\eta^2\partial\xi^2}+\frac{\delta_0}{(1+\eta\delta_0)}\frac{1}{\gamma^2}\frac{\partial^3\psi}{\partial\xi^2\partial\eta}$$

$$-\frac{2\lambda\delta_0^2}{\sqrt{2\delta}}(1+\eta\delta_0)\frac{\lambda^2-2(1+\eta\delta_0)^2}{\left\{(1+\eta\delta_0)^2+\lambda^2\right\}^{5/2}}\frac{\partial v}{\partial\eta}-\frac{2\lambda\delta_0}{\sqrt{2\delta}}\frac{(1+\eta\delta_0)^2}{\left\{(1+\eta\delta_0)^2+\lambda^2\right\}^{3/2}}\frac{\partial^2 v}{\partial\eta^2}+\frac{2\lambda\delta_0^3(1+\eta\delta_0)^2}{\sqrt{2\delta}}$$

$$\frac{2\lambda^2-3(1+\eta\delta_0)^2}{\left\{(1+\eta\delta_0)^2+\lambda^2\right\}^{7/2}}v+\frac{2\lambda\delta_0^2}{\sqrt{2\delta}}\frac{(1+\eta\delta_0)^3}{\left\{(1+\eta\delta_0)^2+\lambda^2\right\}^{5/2}}\frac{\partial v}{\partial\eta}-\delta_0^2\left(\frac{\partial^2\psi}{\partial\eta^2}-\frac{\delta_0}{(1+\eta\delta_0)}\frac{\partial\psi}{\partial\eta}\right)\frac{\lambda^2-(1+\eta\delta_0)^2}{\left\{(1+\eta\delta_0)^2+\lambda^2\right\}^2}$$

$$-\frac{\delta_0(1+\eta\delta_0)}{(1+\eta\delta_0)^2+\lambda^2}\left[\frac{\partial^3\psi}{\partial\eta^3}-\frac{2\delta_0}{(1+\eta\delta_0)}\frac{\partial^2\psi}{\partial\eta^2}+\frac{2\delta_0^2}{(1+\eta\delta_0)^2}\frac{\partial\psi}{\partial\eta}-\frac{\lambda^2\delta_0^2}{(1+\eta\delta_0)^2}\frac{3(1+\eta\delta_0)^2+\lambda^2}{\left\{(1+\eta\delta_0)^2+\lambda^2\right\}^2}\frac{1}{\gamma^2}\frac{\partial^2\psi}{\partial\xi^2}\right]$$

$$-\frac{\lambda^2\delta_0}{(1+\eta\delta_0)\left\{(1+\eta\delta_0)^2+\lambda^2\right\}}\frac{1}{\gamma^2}\left(\frac{\partial^3\psi}{\partial\eta\partial\xi^2}-\frac{\delta_0}{(1+\eta\delta_0)}\frac{\partial^2\psi}{\partial\xi^2}\right) \qquad (7)$$

The boundary conditions for v and ψ are given by

$$v(\pm1,\zeta)=v(\eta,\pm1)=\psi(\pm1,\zeta)=0\,,$$

$$\frac{\partial\psi}{\partial\eta}(\pm1,\zeta)=\psi(\eta,\pm1)=\frac{\partial\psi}{\partial\zeta}(\eta,\pm1)=0\,. \qquad (8)$$

3. Flux through the Helical Duct

To calculate the flux, due to the non-orthogonality of the co-ordinate system, care should be taken about the axial velocity v', which is not perpendicular to $r'-t'$ plane of the helical pipe, where the flow passes through, except at the centerline. The dimensional total axial velocity, Q' through the $r'-t'$ plane is obtained as:

$$Q' = \int_{-b''}^{b''}\int_{-a}^{a} v_n' \, dr dt = \upsilon a Q$$

where, v_n' is the component of the velocity normal to plane and $r'-t'$ plane and

$$Q = \int_{-\gamma\sqrt{(1+\lambda^2)}}^{\gamma\sqrt{(1+\lambda^2)}}\int_{-1}^{1} \frac{1+\eta\delta_0}{\sqrt{(1+\eta\delta_0)^2+\alpha^2\delta_0^2}} v \, d\eta dt$$

is the dimensionless total axial velocity.

The dimensional mean axial velocity $\bar{v}'$ is defined as:

$$\bar{v}' = \frac{Qv}{4\alpha\gamma\sqrt{2\delta}}$$

and the Reynolds number, R_e is:

$$R_e = \frac{\bar{v}'(2a)}{\upsilon} = \frac{Q}{2\gamma\sqrt{2\delta}}.$$

4. Method of Numerical Calculations

The method adopted in the present numerical calculation is the spectral method, in which variables are expanded in series of functions consisting of the Chebyshev polynomials. That is, $v(\eta,\zeta)$ and $\psi(\eta,\zeta)$ are expressed as

$$v(\eta,\zeta) = (1-\eta^2)(1-\zeta^2)\sum_{m=0}^{M}\sum_{n=0}^{N} v_{mn} T_m(\eta) T_n(\zeta)$$

$$\psi(\eta,\zeta) = (1-\eta^2)^2(1-\zeta^2)^2\sum_{m=0}^{M}\sum_{n=0}^{N} \psi_{mn} T_m(\eta) T_n(\zeta)$$

which satisfy the boundary conditions at $\eta = \pm 1$ and $\zeta = \pm 1$. The constants *M* and *N* are the truncation numbers in η and ζ directions, respectively. T_m and T_n are the m[th] and n[th] order Chebyshev polynomial, and v_{mn} and ψ_{mn} are expansion coefficients to be obtained. We substitute these expansions into equations (6) and (7) and apply the collocation method, then we obtain the non-linear algebraic equations for v_{mn} and ψ_{mn}. The collocation points are taken to be

$$\eta_i = \cos\frac{\pi i}{M+2}\ ,\ \zeta_j = \cos\frac{\pi j}{N+2}$$

where *i=1,2,…….,M+1 and j=1,2,…….,N+1.* The obtained non-linear algebraic equations are solved by iterated method and the convergence is assured by taking $\varepsilon_p \langle 10^{-10}$, where subscript *p* denotes the iteration number and ε_p is defined as

$$\varepsilon_p = \sum\sum\left[\left(v_{mn}^{(p+1)} - v_{mn}^{p}\right)^2 + \left(\psi_{mn}^{(p+1)} - \psi_{mn}^{p}\right)^2\right].$$

The basic equations (6) and (7) and the boundary conditions (8) allow us to get a non-symmetric solution with respect to the horizontal line passing through the center of the cross- section. We shall

impose the symmetric condition for the solution. Actually, only non- symmetric solution is obtained due to non-orthogonal helical coordinate system. For sufficient accuracy, we have considered *M=16* and *N=16* in the present numerical calculations.

5. Results and Discussion

5.1. Comparison

The detailed comparisons on the flow through a curved duct (torsion parameter, $\lambda = 0$) with aspect ratio, $\gamma = 1$ (square cross-section) and non-dimensional curvature $\delta = 0.02$ are presented here. First, present values of the Dean number may be compared at the limit points L_1 and L_2 with those of Winters's(1987). Winters has shown the results at the pressure gradient instead of the Dean number, but these can be related by: $q = \frac{D_n}{\sqrt{2\delta}}$, where q is the axial pressure gradient in Winters's notation.

Table 1. Comparison of the Dean numbers at the limit points

Limit points	D_n (Present)	D_n (Winters)
L_2	683.0109491015334	683.26
L_1	579.0281357122883	579.25

Table 1 shows the comparison of present result with those of Winters's by considering the truncation number (M, N)=(16,16). It is seen that present results show a good agreement with Winters's results. Present ones are more precise than those of Winters's and his calculations yield rather good results for the values of L_1 and L_2 in such simple flows.

However, the spectral method with Chebyshev polynomial expansion as well as Rahpson method for iteration generally has the superiority to the other methods in numerical accuracy to solve differential equations in a closed domain and it is the most suitable method for the present problem containing complex flow structures. Therefore, it may be expected that the present numerical calculations give the flow characteristics accurately.

5.2. Helical pipe with large aspect ratio

Some numerical calculations have been made of Dean numbers D_n=50 & 100 for different aspect ratio γ and torsion parameter λ at dimensionless curvature $\delta = 0.1$. Therefore, interesting flow behavior will be expected if the helical duct with large aspect ratio is involved. It is also expected that the present numerical results measure better flow characteristics, although the multiple solutions may not be obtained. However, we have obtained multiple solutions in curved duct with large aspect ratio as well as in square cross section (Alam et al., 2006). Yamamoto et al. (1999) presented some results in case of square cross-section and did not produce any multiple solutions or bifurcation diagram. For different values of torsion, Fig. 2 shows the vector plot of the secondary flow in a cross-section while the streamlines plots at $D_n = 50$ are shown in Fig. 3 and also Fig. 4 shows the equi-velocity lines of the axial flow at $D_n = 50$. For each figure the outer wall is to the right and the inner wall is to the left. The length of arrow indicates the ratio of the stream velocity to the axial velocity and the direction of the flow in vector plots are always indicated by an arrowhead, no matter how small the flow is. Thus, the relative strength of the flow is not resolved for areas of a very weak secondary flow.

For a helical duct with finite pitch and aspect ratio, $\gamma \geq 1$ no symmetric solution can be expected. A pair of vortex locates upper and lower with unequal size but opposite direction of rotation with respect to the symmetric line through the centers of the duct and the curvature (see Figs. 2 & 3). The vortex rotating in the counter-direction of torsion (the upper vortex rotating anti-clockwise) is weakened and shifted to the upper right of the cross-section if we impose torsion force. On the other hand, the other

vortex rotating in the same direction of torsion (lower vortex rotating clockwise) is strengthened and

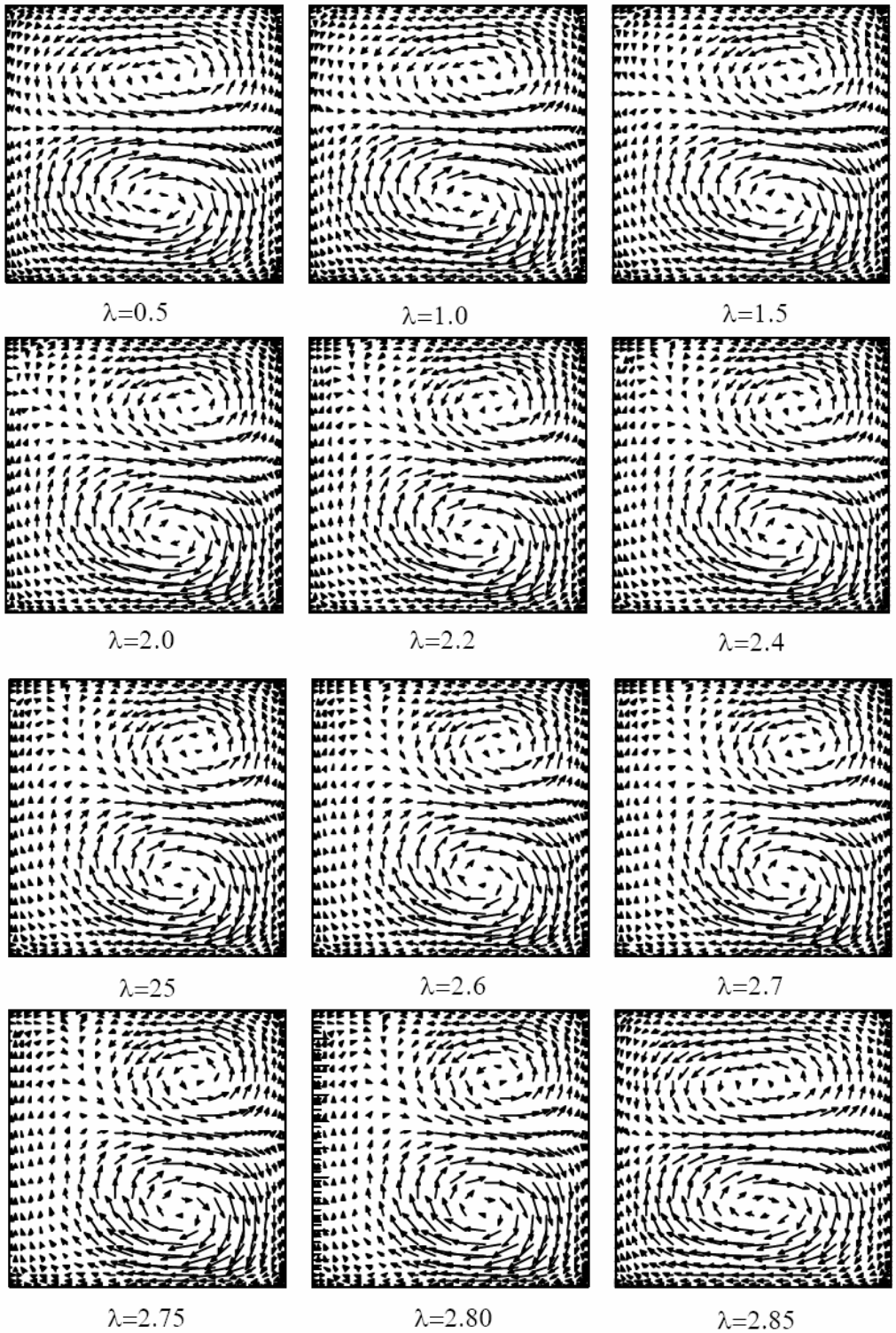

Fig. 2 Vector plots of the secondary flow for helical square duct at different values of λ with δ =0.1 and Dn=50, outside is to the right.

shifted to the lower right of the cross-section (see Fig. 2 & 3). At Dean number 50, a characteristic feature for increasing torsion is that the lower vortex of the secondary flow expands with the reduction

of the upper vortex. This can be seen in vector plots of Fig. 2 and the streamline plots of Fig. 3. The qualitative behavior is experimentally reported by Bolinder and Sunden(1995) for helical pipe with square cross-section as shown in Fig. 5(a) & 5(b). The effect of torsion on the axial flow is minor for ducts of low moderate pitch (Fig. 4). The maximum axial flow shifts to the lower half of the cross section. If the torsion is increased further, the location of the maximum axial flow moves to the lower right side corner of the cross-section.

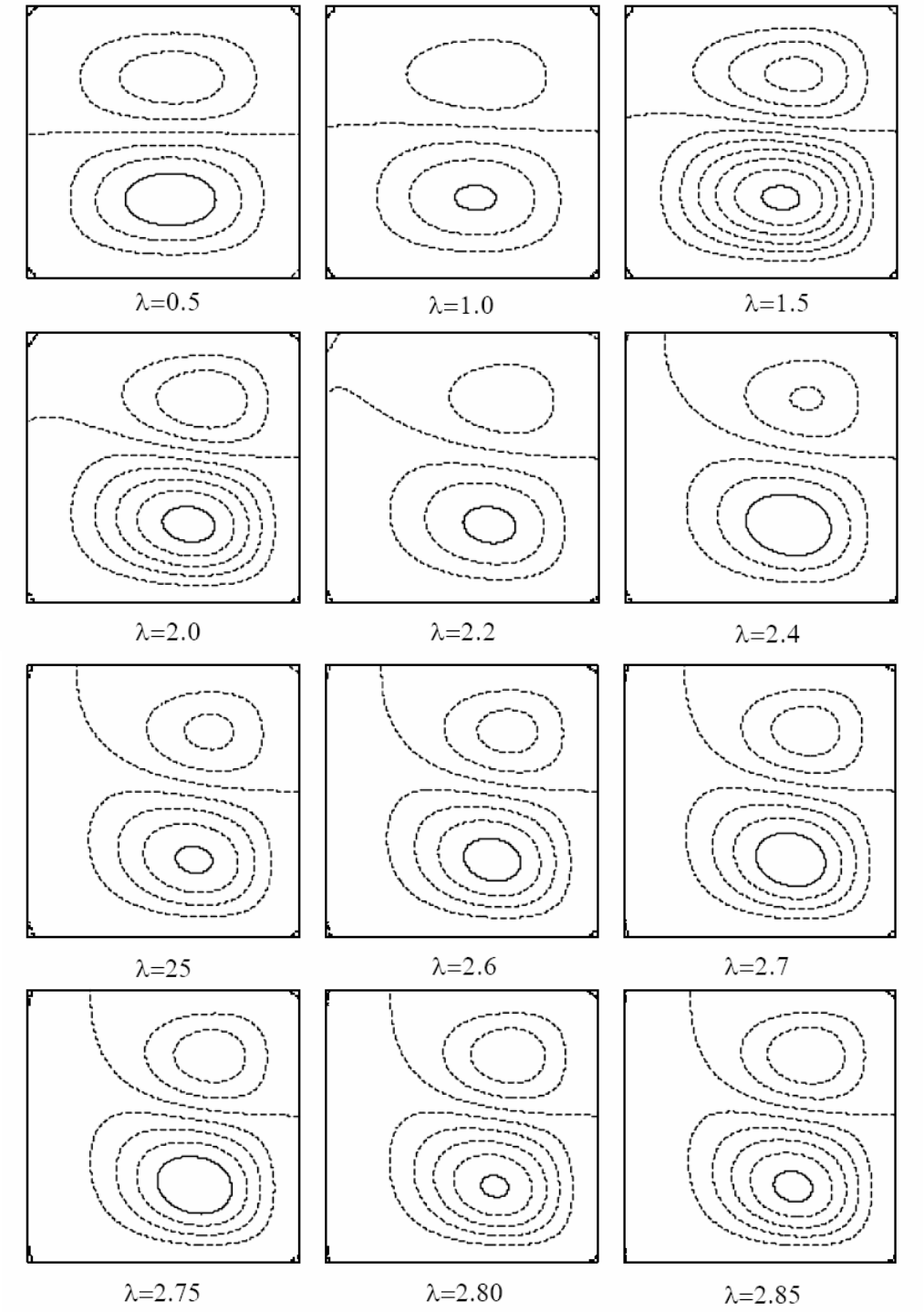

Fig. 3 Streamline plots of the secondary flow for helical square duct at different values of λ with δ=0.1 and Dn=50, outside is to the right

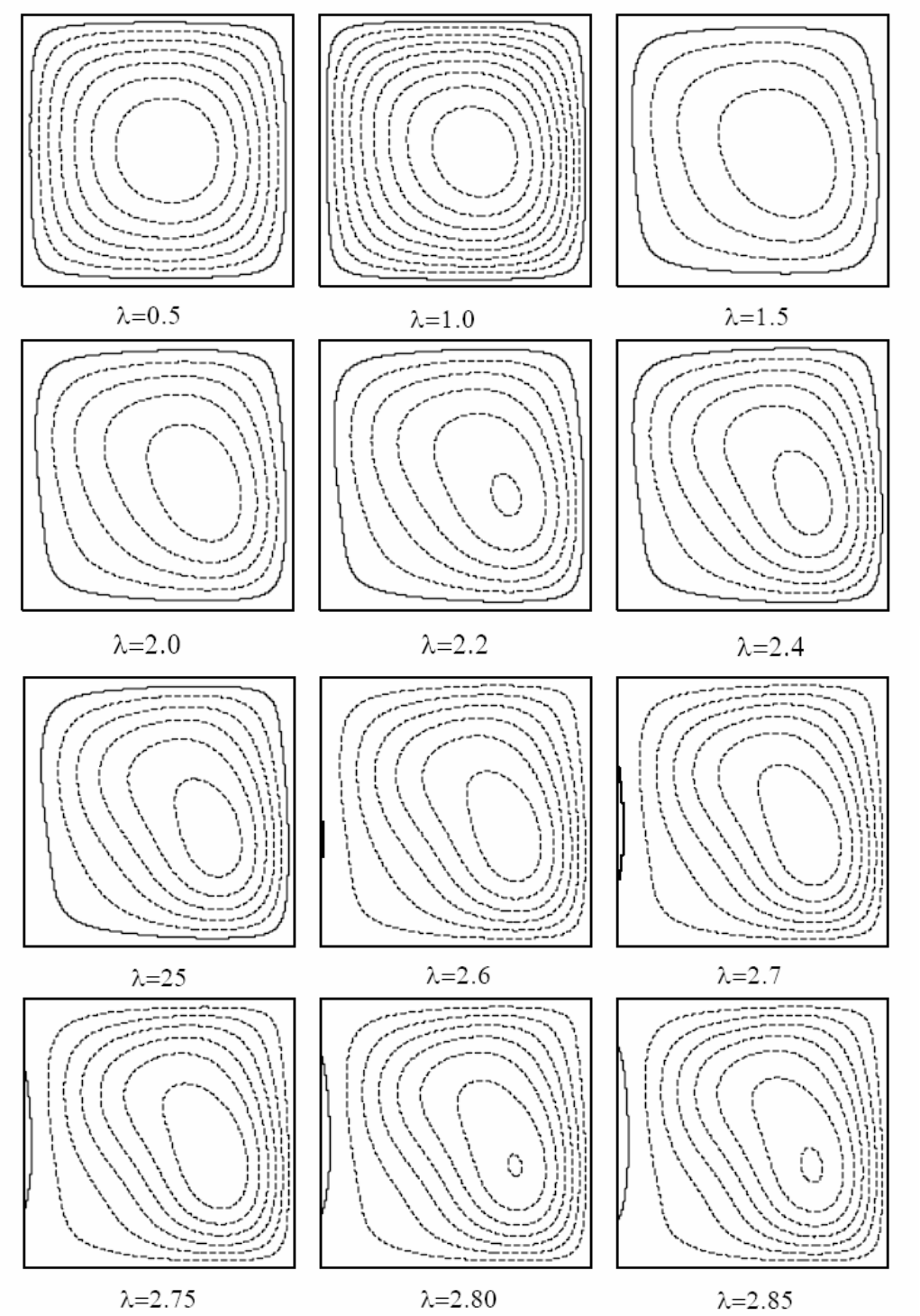

Fig. 4 Contour plots of the axial flow for helical square duct at different values of λ with δ = 0.1 and Dn = 50, outside is to the right

Here is a brief note on the flow through a rectangular helical duct with large aspect ratio $1.0 \le \gamma \le 2.4251$ and non-dimensional curvature $\delta = 0.1$ at dean number $Dn = 100$. This Dean number is chosen because that is considered to be representative showing high flow patterns in the

helical curved duct. In this work, the iterative method is utilized for solving the obtained algebraic non-linear equations. In Figs. 6 & 7, two-cell structure of secondary flow patterns are obtained at aspect ratio $\gamma = 1.0$ and these are not symmetric. There is not that much change in the flow pattern at the aspect ratios $1.0 \le \gamma \le 2.4251$. Only the upper vortex is reduced and lower vortex is expanded. The maximum axial flow at the horizontal centerline of the pipe is shifted towards the high-pressure side of the pipe as shown in Fig. 8.

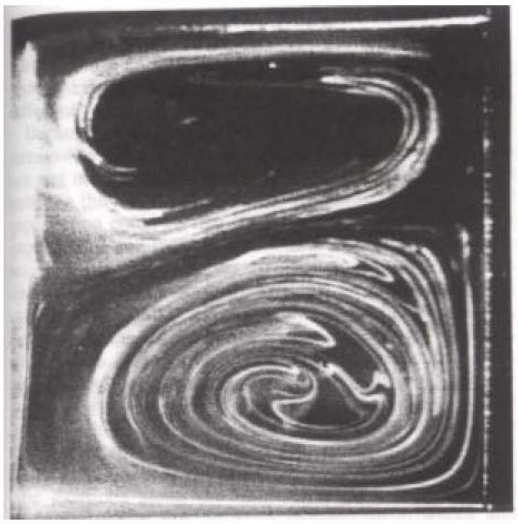

Fig. 5(a) Experimental result

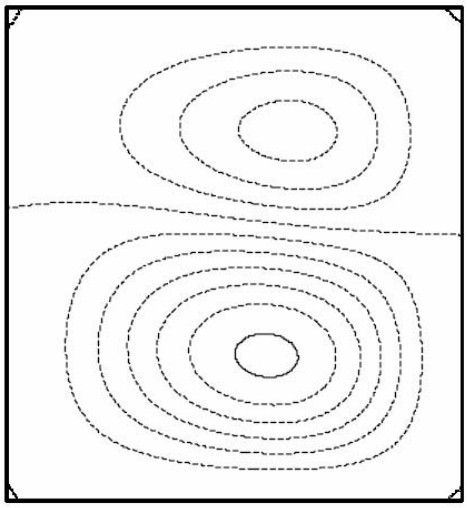

Fig. 5(b) Numerical result

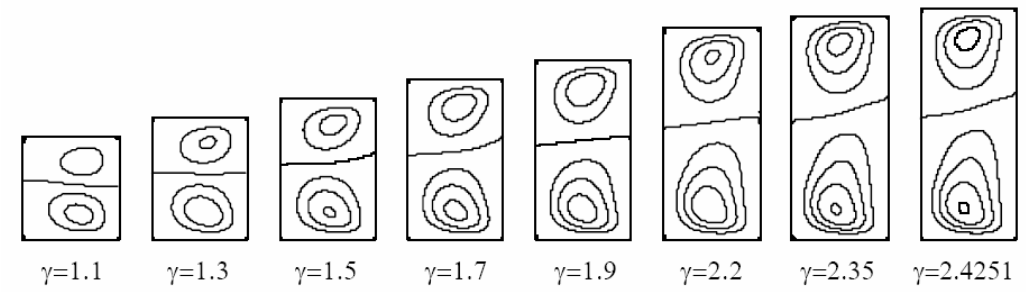

Fig. 6 Stream line plots of the secondary flow at different values of aspect ratio with λ=2.0 and Dn=100

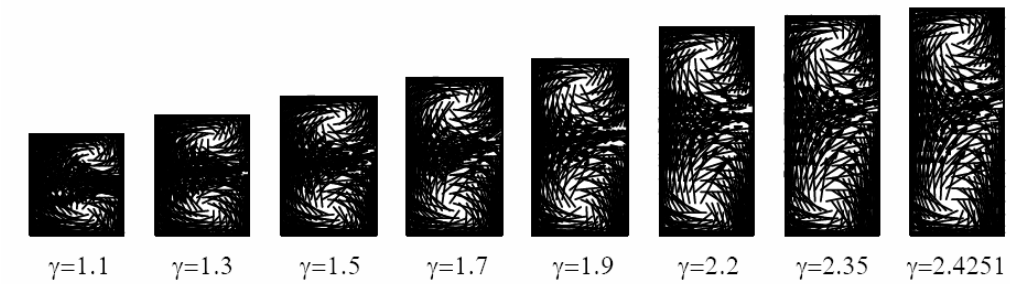

Fig. 7 Vector plots of the secondary flow at different values of aspect ratio with λ=2.0 and Dn=100

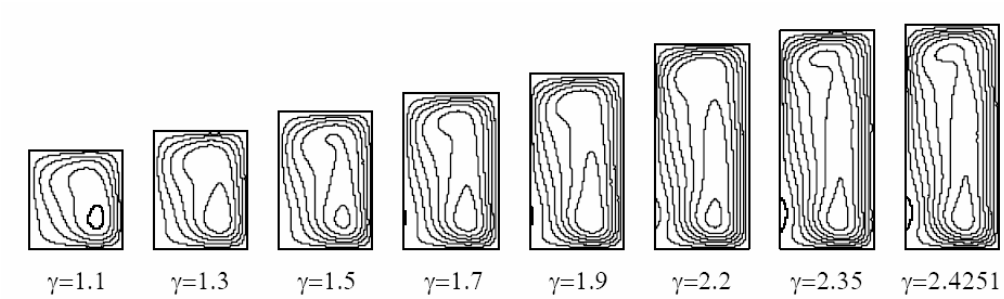

Fig. 8 Contour plots of the axial flow at different values of aspect ratio with λ=2.0 and Dn=100

The physical mechanism responsible for such behavior is easily understood once we recognize that the curvature has the tendency to induce a secondary flow (without torsion) directed radially outward in the middle of the channel, while the torsion has a tendency to induce a secondary flow in radially inward direction.

6. Conclusions

Flow through a helical pipe with rectangular cross-section is studied in this research. From the above results and discussions, following conclusions can be drawn:

1. The multiple solutions have not been obtained in case of helical pipe with rectangular cross-section and for finite pitch no symmetric solution can be expected.
2. A pair of vortex of the secondary flow locates upper and lower with unequal size but opposite direction of rotation with respect to the symmetric line through the centers of the duct and the curvature.
3. If the torsion is increased, the lower vortex of the secondary flow expands with the reduction of the upper vortex and the location of the maximum axial flow moves to the lower right side corner of the cross-section.
4. The maximum axial flow at the horizontal centerline of the pipe is shifted towards the high-pressure side of the pipe.

References

Alam, M. M., Begum, D, Islam, N. and Yamamoto, K. and (2006): Multiple Solution of a Flow in a Curved Rectangular Duct With Large Aspect Ratio, Journal of Energy Heat and Mass Transfer, 28, 181-301.

Bolinder, C. J. and Sunden, B. (1995): Flow Visualization and LDV Measurements of Laminar Flow in A Helical Square Duct With Finite Pitch, Experimental thermal and fluid science, 11, 348-363. doi:10.1016/0894-1777(95)00040-2

Cheng, K. C., Lin, R. and Ou, J. W. (1976): Fully Developed Laminar Flow in Curved Rectangular Channels, ASME Journal of Fluids Engineering, 98, 41-48.

Chen, W. H. and Fan, C. N. (1986): Finite element Analyses of Incompressible Viscous Flow in a Helical Pipe, Computational Mechanics, 1, 281-292.

Ghi, K. N. and Sokhey, J. S.(1977): Laminar Incompressible Viscous Flow in Curved Ducts of Rectangular Cross-section, ASME Journal of Fluids Engineering, 99, 640-648.

Joseph, B., Smith, E. P. and Adler, R. J. (1975): Numerical Treatment of Laminar Flow in Helical Coiled Tubes of Square Cross Section, AIChE Journal, 21, 965-979. doi:10.1002/aic.690210519
Kao, H. C. (1987): Torsion Effect on Fully Developed Flow in a Helical Pipe, Journal of Fluid Mechanics, 184, 335-356. doi:10.1017/S002211208700291X

Manlapaz, R. L. and Churchill, S. W. (1980): Fully Developed Laminar Flow in a Helical Coiled Tube of Finite Pitch, Chemical Engineering Communications, 7, 57-78. doi:10.1080/00986448008912549

Murata, S., Miyake, Y., Inaba, T. and Ogawa, H.(1981): Laminar Flow in a Helical Coiled Pipe, Bulletin of the JSME, 24, 355-362.

Winters, K. H.(1987): A Bifurcation Study of Laminar Flow in a Curved Tube of Rectangular Cross-Section, Journal of Fluid Mechanics, 180, 343-369. doi:10.1017/S0022112087001848

Wang, C. Y.(1981): On The Low-Reynolds-Number Flow in a Helical Pipe, Journal of Fluid Mechanics, 108, 185-194. doi:10.1017/S0022112081002073

Xie, D. E. (1990): Torsion Effect on Secondary Flow in a Helical Pipe, International Journal of heat and fluid flow, 11, 114-119. doi:10.1016/0142-727X(90)90004-U

Yamamoto, K., Alam, M. M., Yasuhara, J. and Aribowo, A. (2000): Flow Through a Rotating Helical Pipe with Circular Cross Section, International Journal of Heat and Fluid Flow, vol. 21, 213-220. doi:10.1016/S0142-727X(99)00079-X

Yamamoto, K., Yanase, S. and Alam, M. M. (1999): Flow Through a Rotating Curved Duct With Square Cross Section, Journal of the physical society of Japan, vol. 68(4), 1173-1184. doi:10.1143/JPSJ.68.1173